# 3D hydrodynamic modelling of a microtidal barred beach (Sète, NW Mediterranean Sea) during storm conditions

Heloise Michaud, Nicolas Robin, C. Estounel, Patrick Marsaleix, Yann Leredde, R. Certain, Frederic Bouchette

# 3D HYDRODYNAMIC MODELLING OF A MICROTIDAL BARRED BEACH (SETE, NW MEDITERRANEAN SEA) DURING STORM CONDITIONS

Héloïse Michaud[1,2,3], Nicolas Robin[4], Claude Estournel[3], Patrick Marsaleix[3], Yann Leredde[2], Raphaël Certain[4] and Frédéric Bouchette[2]

## Abstract

The field campaign on the Sète coast deployed during the winter 2009 was used to understand the hydrodynamics on a double barred beach in the surf zone during storm periods. The large set of measurements collected at several position and depth were also useful to improve the 3D circulation model Symphonie that takes into account the atmospherics and wave forcings. Once implemented on the beach and supplemented with some additional parameterizations concerning the roller effects and the bottom friction, the model was tuned and validated in the surf zone. The role of the different processes was then analysed. Thus, the roller and the bottom friction are of primary importance in the dynamics of the circulation. Thanks to its 3D nature and once associated with a sediment transport model and a morphodynamic model, Symphonie will offer a good representation of the sediment transport.

**Key words:** hydrodynamics, waves, current, 3d model, measurements

## 1. Introduction

The study area (Sète beach) is located on the Languedoc-Roussillon coast in the Gulf of Lion (southern part of the French Mediterranean coast) (figure 1). The nearshore zone is composed by two straight sandy bars which control the transformation and the dissipation of waves that propagate to the shoreline. They also control the swash, the run-up and partly the changes of the water level in the nearshore zone. This microtidal environment is classified as wave-dominated coast despite a low storm frequency. However, these energetic periods have a high morphogenic power for the system and for the coastline evolution (Certain, 2002). As the major part of the world coast, the study area presents intensive erosion due to human impact and a decrease of the sedimentary stock. Thus, for an integrated management approach of coastal hazard in a high socio-economic context, it appears necessary to increase our knowledge on hydrodynamic processes that occur in these environments during storm conditions. It can be achieve with in-situ measurements and numerical modeling and this is the first objective of this paper.

For years, the strategy to model hydrodynamics on such nearshore barred system has relied on nonlinear depth-averaged approaches, from the pioneer work of Longuet-Higgins and Stewart (1962) to recent and innovative approaches based on the Green-Naghdi formalism (e.g. Bonneton et al. 2011). Recently developed 3D wave-current interaction theories (e.g., McWilliams et al. 2004, Ardhuin et al. 2008) have provided useful approaches that have been implemented in Boussinesq hydrostatic 3D circulation models (e.g. Denamiel 2006, Uchiyama et al. 2010, Bennis et al. 2011), and in particular in the Symphonie model (Marsaleix et al. 2006, 2008, 2009; Michaud et al. 2012). In Michaud et al. (2012), Symphonie has reproduced the circulation in the Mediterranean Sea during a storm period at the inner shelf scale, and has been tested in the surf zone only in academic cases. Between 15 December 2008 and 25 February 2009, a

[1]SHOM, 42 Avenue Gaspar Coriolis, Toulouse 31057, France. heloise.michaud@shom.fr
[2]UMR Géosciences Montpellier, Université Montpellier 2, CNRS, place Eugène Bataillon, 34095 Montpellier cedex 5, France. yann.leredde@um2.fr, frederic.bouchette@um2.fr
[3]UMR Laboratoire d'Aérologie, Université de Toulouse, CNRS, 14, Avenue Edouard Belin, 31400 Toulouse, France. estc@aero.obs-mip.fr, marp@aero.obs-mip.fr
[4]UMR CEFREM, University of Perpignan, 52 Avenue Paul Alduy, Perpignan 66860, France. Nicolas.robin@univ-perp.fr, raphael.certain@univ-perp.fr

field campaign with several instruments measuring wave, current and water level parameters was conducted on the Sète beach. At least, three storms occurred on this period. By implementing typical nearshore processes like the roller effect and with the support of the measurements, the second objective of this study is to improve the Symphonie model, so it can be deployed successfully at the nearshore scale, in realistic conditions.

The paper is organized as follows: the experimental setup and the numerical models are presented in section 2. Then, section 3 describes the measurements and the result of the simulation during the storm period. Section 4 proposes some discussions and sensitivity tests on the roller and on the bottom stress to understand the physical processes responsible of the solution, and a conclusion is presented in section 5.

## 2. **Material and methods**

### 2.1. *Instrumental devices*

The study zone is located on the south of France along Languedoc-Roussillon coasts, between Marseillan and Sète. Several instruments measuring wave, current and water level parameters at several depths were deployed on the Sète beach (figure 1a), on a transect perpendicular to the shoreline (figure 1b) (Robin et al., 2010).

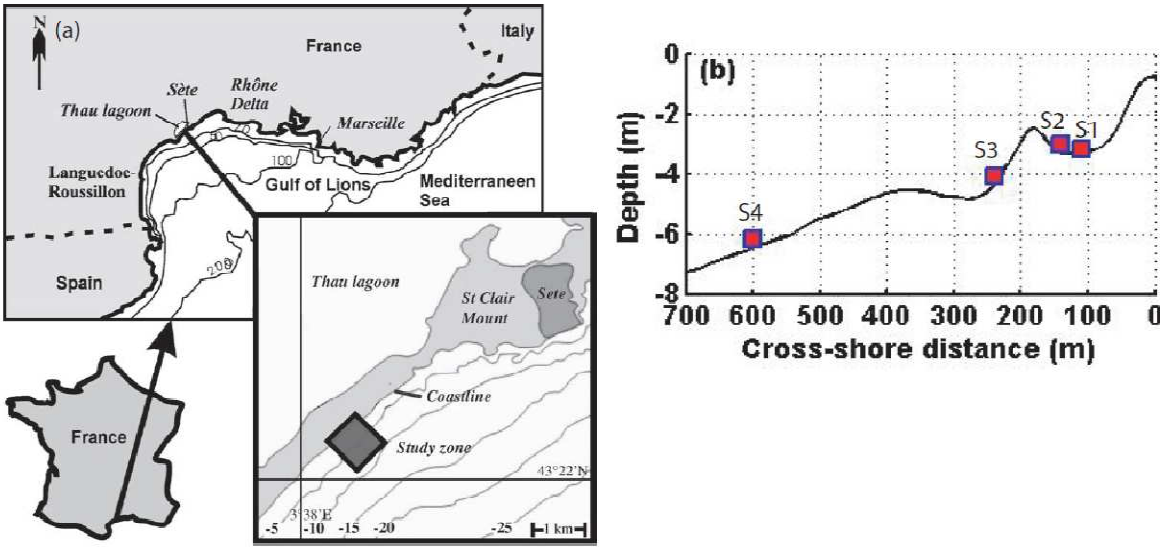


Figure 1. Location of the study zone (extracted from Certain et al., 2005) (a) and beach profile and location of the four stations (b).

Table 1. Characteristics of the instruments

| **Instruments** | Location | Current burst length | Wave burst length | Recording frequency |
|---|---|---|---|---|
| **Nortek ADV** | two adv at two different depths at S1 and one adv at S1 and S3 | 20 min/2h40 | 20min/3h | 2Hz |
| **RDI ADCP** | S2 | 1min/3min | 20min/3h | 2Hz |
| **RDI ADCP** | S3 | 1min/6min | 20min/3h | 2Hz |
| **Interocean current meter** | S4 | 20min/3h | 20min/3h | 2Hz |

The instruments were positioned at four locations of the transect: two stations in the inner trough (S1 and S2 located respectively at 65 m and 95 m of distance from the shoreline and at 3.15 m and 3.3 m of water

depth), one on the seaward side of the inner bar (S3 at 185 m of distance and under 4.25 m of water depth) and one on the lower shoreface (S4 at 600 m from the shoreline and under 6.65 m of water depth). The instrumental devices are composed of 4 Nortek ADV (Acoustic Doppler Velocimeter) (two at S1, one at S2 and S3 which record the bottom current and pressure sensor), two RDI 600kHz ADCP (Acoustic Doppler Current Profiler) located at S2 and S3 and one Interocean current meter with wave sensor at S4. The characteristics and sampling rates of the instruments are described in Table 1.

### 2.2. *Numerical models and implementation*

2.1.1. *Circulation model*

The Boussinesq hydrostatic 3D circulation model Symphonie is used to reproduce the circulation on the double barred beach. This model has been extensively used in studies of the Mediterranean Sea and in particular along the Languedoc coasts (Denamiel, 2006, Leredde et al. 2007, Michaud et al. 2013), generally comparing satisfactorily with available in situ observations.

Components of currents, temperature and salinity are computed on a C-grid using an energy conserving finite difference method. Vertical mixing is parameterized according to the k-ε turbulent closure scheme. Recent developments in the Symphonie model have integrated the wave-induced currents as described in Michaud et al. (2012). The wave-induced current theory follows the simplified equations of Bennis et al. (2011) based on the glm2z-RANS theory Ardhuin et al. (2008). These adiabatic equations are completed by additional parameterizations of wave breaking, wave streaming on the bottom and wave-enhanced vertical mixing. Thus the evolutions of the quasi-Eulerian velocities $(\hat{u}, \hat{v}, \hat{w})$ are governed by:

$$\begin{cases} \frac{\partial \hat{u}}{\partial t} + \underbrace{\hat{u}\frac{\partial \hat{u}}{\partial x} + \hat{v}\frac{\partial \hat{u}}{\partial y} + \hat{w}\frac{\partial \hat{u}}{\partial z}}_{advection} \underbrace{-f\hat{v}}_{coriolis} + \underbrace{\frac{1}{\rho}\frac{\partial p^H}{\partial x}}_{pressure\ gradient} = \underbrace{fV_s}_{Stokes\ Coriolis} \\ \underbrace{+(\frac{\partial \hat{v}}{\partial x} - \frac{\partial \hat{u}}{\partial y})V_s - W_s\frac{\partial \hat{u}}{\partial z}}_{vortex} \underbrace{-\frac{\partial (S^J + S^{shear})}{\partial x}}_{bernoulli\ pressure\ head} + \underbrace{F_{m,x}}_{mixing} + \underbrace{F_{d,x}}_{wave\ dissipation} \\ \frac{\partial \hat{v}}{\partial t} + \underbrace{\hat{u}\frac{\partial \hat{v}}{\partial x} + \hat{v}\frac{\partial \hat{v}}{\partial y} + \hat{w}\frac{\partial \hat{v}}{\partial z}}_{advection} \underbrace{+f\hat{u}}_{coriolis} + \underbrace{\frac{1}{\rho}\frac{\partial p^H}{\partial y}}_{pressure\ gradient} = \underbrace{-fU_s}_{stokes\ coriolis} \\ \underbrace{+(\frac{\partial \hat{v}}{\partial x} - \frac{\partial \hat{u}}{\partial y})U_s - W_s\frac{\partial \hat{v}}{\partial z}}_{vortex} - \underbrace{\frac{\partial (S^J + S^{shear})}{\partial y}}_{bernoulli\ pressure\ head} + \underbrace{F_{m,y}}_{mixing} + \underbrace{F_{d,y}}_{wave\ dissipation} \end{cases} \quad (1)$$

$(u, v, w)$ are the mean Lagrangian velocities and (Us, Vs, Ws) the Stokes velocities in the horizontal ($x$,y) and vertical (z) directions. They are valid from the bottom z=-h to the local phase-averaged free surface z=$\hat{\eta}$. $p^H$ is the hydrostatic pressure, $f$ the Coriolis parameter, $\rho$ the mean density and $t$ the time.

The forces added by the wave forcing in the momentum equations are: the Stokes-Coriolis force, the force linked to the wave-induced and shear-induced mean pressure called the Bernoulli pressure head, the mixing force where some parameterizations of the wave-enhanced mixing are taken into account, the vortex force and the force of wave dissipation by breaking and bottom dissipation ($\overrightarrow{F_d} = \overrightarrow{F_d^{surf}} + \overrightarrow{F_d^{bottom}}$). However, we choose to include the force linked to wave dissipation by bottom friction is in the bottom boundary conditions as a bottom stress.

$$\begin{cases} K_z \frac{\partial \hat{u}}{\partial z}\Big|_{z=-h} = \tau_{bot,x} + \tau_{wob,x} \\ K_z \frac{\partial \hat{v}}{\partial z}\Big|_{z=-h} = \tau_{bot,y} + \tau_{wob,y} \end{cases} \quad (2)$$

$K_z$ is the vertical eddy viscosity, $\overrightarrow{\tau_{bot}} = (\tau_{bot,x}, \tau_{bot,y})$ is the bottom stress linked to current and $\overrightarrow{\tau_{wob}} = (\tau_{wob,x}, \tau_{wob,y})$ is the momentum lost by wave due to bottom friction. This momentum is responsible for the streaming flow. Three different parameterizations of bottom stress $\overrightarrow{\tau_{bot}}$ are implemented in the model.

- The first one is a quadratic bottom drag parameterization and is only linked to the current through:

$$\overrightarrow{\tau_{bot}} = \rho \left( \frac{\kappa}{\ln(z_1/z_0)} \right)^2 \|\overrightarrow{V_b}\| \overrightarrow{V_b} \quad (3)$$

Where $z_0$ is a length scale representing the roughness of the bottom boundary and $z_1$ is the distance between the first level above the bottom boundary and the bottom boundary. $\overrightarrow{V_b}$ is the near bottom current and $\kappa$=0.4 the Von Karman constant.

- The second one is a linear bottom drag parameterization (with $\mu$ a linear drag coefficient) :

$$\overrightarrow{\tau_{bot}} = \rho \mu \overrightarrow{V_b} \quad (4)$$

- The third one is a drag law function linked to waves and currents, established by Soulsby et al. (1995):

$$\overrightarrow{\tau_{bot}} = \overrightarrow{\tau_c} \left[ 1 + 1.2 \left( \frac{|\tau_w|}{|\tau_w| + |\overrightarrow{\tau_c}|} \right)^{3.2} \right] \quad (5)$$

$\overrightarrow{\tau_c}$ is the bottom stress due to current only and $\tau_w$ is the bottom stress linked to waves only, are given by:

$$\begin{cases} \overrightarrow{\tau_c} = \rho \left( \frac{\kappa}{\ln(z_1/z_0)} \right)^2 \|\overrightarrow{V_b}\| \overrightarrow{V_b} \\ |\tau_w| = 0.5 \rho f_w |\overrightarrow{u_{orb}}|^2 \end{cases} \quad (6)$$

$f_w$ is the wave friction factor and $\overrightarrow{u_{orb}}$ the bottom wave orbital velocity. Some parameterizations to calculate these terms are given in Michaud et al. (2012).

Numerous in-situ observations and laboratory measurements (e.g. Svendsen 1984, Ruessink et al. 2001) have shown that models and theories were robust outside the surf zone, but non linearity processes associated to the creation of a roller were important and source of divergence between model and reality, especially in the position of the longshore drift, often predicted too offshore in models (Feddersen et al 1998, Church and Thornton 1993). Thus, some in-situ and laboratory studies (e.g., Apotsos et al. 2007) were initiated in order to characterize the rollers, and their effects on the circulation. We inspire from these works to include the roller effect in our model.

Thus, Stokes velocities are now equal to:

$$(U_s, V_s) = \sigma k (\cos\theta, \sin\theta)(E + E_r) \frac{2\cosh(2k(z+h))}{\cos(2kD)} \quad (7)$$

with D=η+h the water depth, g the acceleration due to gravity, E the wave energy, $E_r$ the roller energy, k the wave number, $\sigma$ the relative frequency and $\theta$ the angle of wave propagation.

The force of breaking dissipation becomes:

$$\overrightarrow{F_d^{surf}} = \frac{\left((1-\alpha_r)\varepsilon^b + \varepsilon^r\right)\vec{k}}{\sigma\rho} \frac{f(z)}{\int_{-h}^{\hat{\eta}} f(z')dz'} \quad (8)$$

$\varepsilon^b$ is the breaking dissipation rate, $\varepsilon^r$ the roller dissipation rate and $\frac{f(z)}{\int_{-h}^{\hat{\eta}} f(z')dz'}$ is a normalized vertical distribution function with $f(z) = \cosh\left(\frac{z+h}{0.64\, H_{sw}}\right)$. $H_{sw}$ is the significant wave height of the wind-sea only. The roller energy $E_r$ is calculated with:

$$\frac{\partial}{\partial x}\left(E_r \cos\theta\, c\right) = -\varepsilon^r + \alpha_r \varepsilon^b \tag{9}$$

with $c$ the phase speed of the primary wave. The roller dissipation rate is given by $\varepsilon^r = \frac{g\, E_r \sin\beta}{c}.\ \sin\beta$, the slope of the roller, is set equal to 0.1 (Reniers et al., 2004). Besides, $\alpha_r$ comprised between 0 and 1, represents the proportion of primary wave that gives its energy to the roller (Tajima et al., 2006, Uchiyama et al., 2010). This term provides a formulation of $E_r$ that can reproduce the different types of breaking and forms of beach.

The bathymetry of the computational domain is created from the bathymetric survey performed on 13 January 2009 on the double barred beach. The domain has the dimension of 860 m in the cross-shore direction x and 60 m in the alongshore direction y. Lateral periodic conditions are stipulated and we consider the shoreline as a wall. At the offshore boundary, we use a Neumann boundary condition. The coast has an orientation of 43° to the north. The maximum water depth is 8 m at the offshore boundary, and the shoreline at rest is set at x=0. The horizontal resolution is 10 m, and there are 30 vertical levels. The bottom roughness length is set to 0.1 mm throughout the domain and we use the wave-current drag model defined by Soulsby et al. (1995). For the reference simulation, we take into account the roller effects with $\alpha_r$ =1. A positive cross-shore velocity is oriented toward the coast and a positive longshore velocity is oriented toward the south-west.

The meteorological forcings (surface pressure, air temperature, relative humidity, wind velocity and radiative fluxes) are taken from the Aladin model every 3 hours (the regional weather forecasting model from Météo-France, which has a resolution of 10 km). A complete description of the bulk formulae used to compute the air/sea fluxes is given in Estournel et al. (2009). The tidal effects are neglected since the beach is located in a highly micro-tidal region.

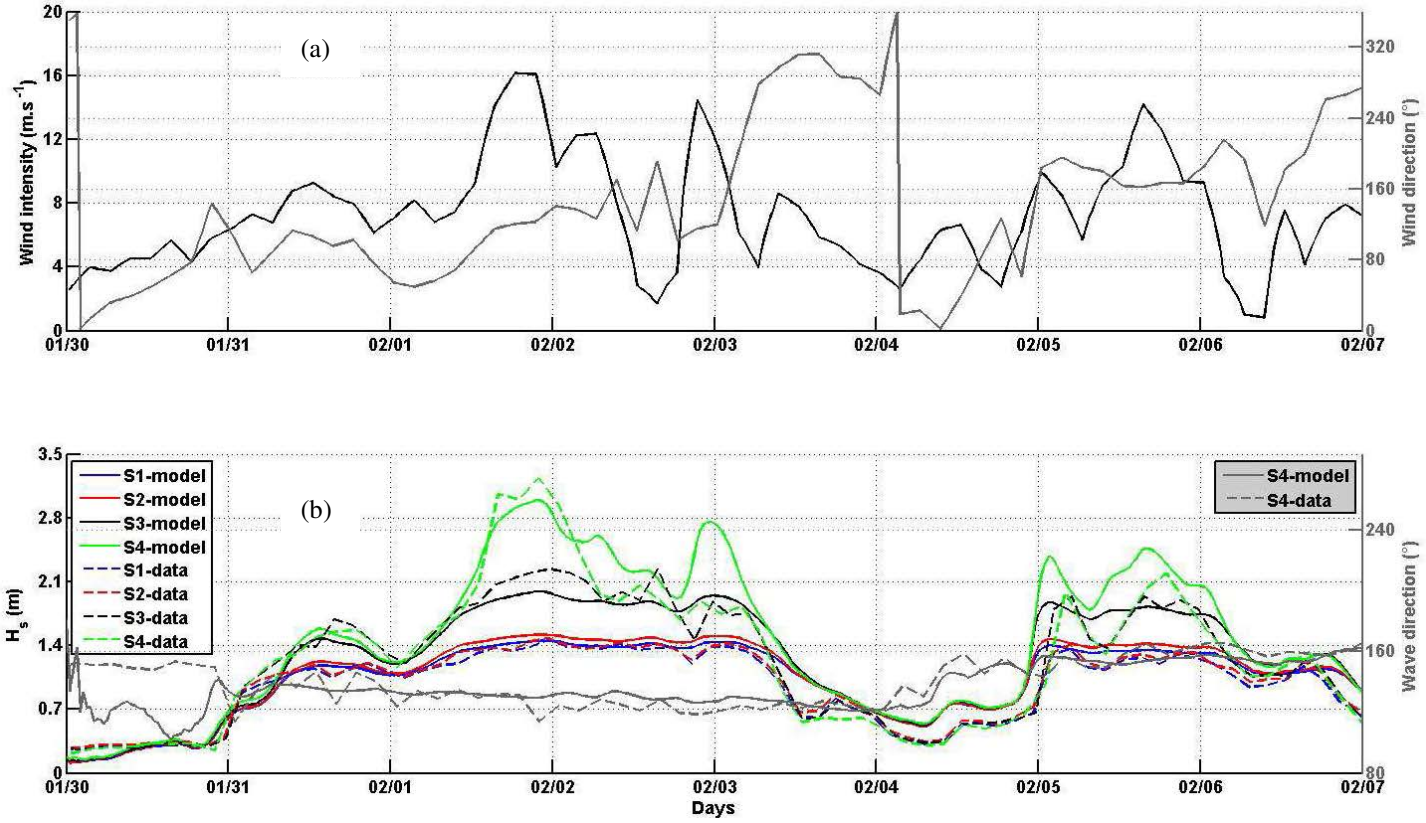


Figure 2.Wind intensity and direction (a) and comparison of the significant wave height at the four locations and the wave direction at S4, between simulation (solid line) and data (dashed line) (b).

2.1.1. *Wave model*

The wave forcing is performed by the wave generation and propagation model Wavewatch III (WW3) (Tolman 2008, Ardhuin et al. 2010). For a correct representation of the sea state at the beach scale with a consistent resolution, we have used five nested grids whose coverages range from the entire West Mediterranean Sea to the beach (with an increasing resolution from 0.1° to 50 m). Simulations are run for the January-February 2009 period. TEST405 parameterizations described in Ardhuin et al. (2010) have been used. The wind velocities are also provided by the Aladin model every 3 hours, except for the MEDOC grid where Aladin is completed by Arpege (a global atmospheric model from Météo-France with a grid resolution of 15 km over France).

## 3. Results

### 3.1. *Measurements during the February storm*

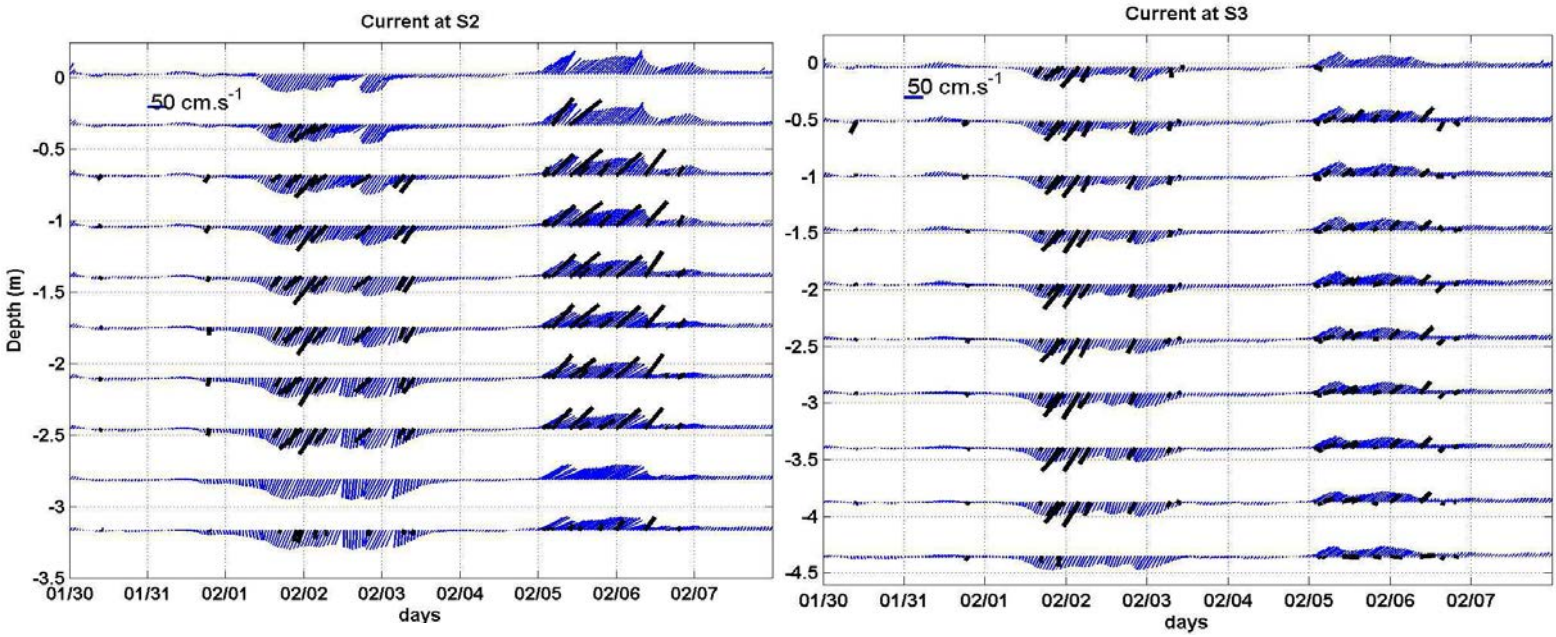


Figure 3.Comparison of current intensities at S2(left) and S3(right) between data (black) and simulation (blue) in function of depth and time. Each stick length represents the current intensity and its angle represents its orientation. A stick oriented to the top means a current directed to the north.

During the field campaign, at least three storms occurred but in this paper, only the February storm is studied. From 1 February 2009, a 7-day sea storm occurred, characterized by a wind coming in the first days from the north-east then from the south-east, reaching 12 $m.s^{-1}$ at the storm apex (figure 2). The significant wave height reaches 3 m at S4, with a period of 7s. Besides, this storm has the originality to be divided in two periods: two peaks with a second one less strong, and a different wave angle of origin: east-south-east then south-east, from 4 February.

A drift directed towards the south-west is measured during the first period of the storm (Figure 3). It is particularly strong in the inner trough (at S2, it reaches 0.93 $m.s^{-1}$) and on the external side of the inner bar (0.8 $m.s^{-1}$ at S3). Then, as a consequence to the change in wave direction, the drift turns towards the north-east on 5 February and is the strongest once again in the inner trough (1 $m.s^{-1}$).

### 3.2. *Reference simulation*

The wave model reproduces quite well the measurements at the four locations (figure 2b) and the decreasing significant height when approaching the coast, due to dissipation by breaking and bottom

friction. The period and the direction are also in agreement with the data. However, some underestimations or overestimations are nevertheless obtained for the significant wave height, for example for S4 on 3 February, with overestimation of 70 cm in the model.

The dissipation of the wave energy is at the origin of a longshore drift that has a maximum intensity on the bars. From 1 to 4 February, the drift is oriented toward the south-west, reaching intensity equal to 0.6 $m.s^{-1}$. Then, as in the measurements, the drift turns oriented toward the north-east, and reaches 0.75 $m.s^{-1}$ in the inner trough on 5 February.

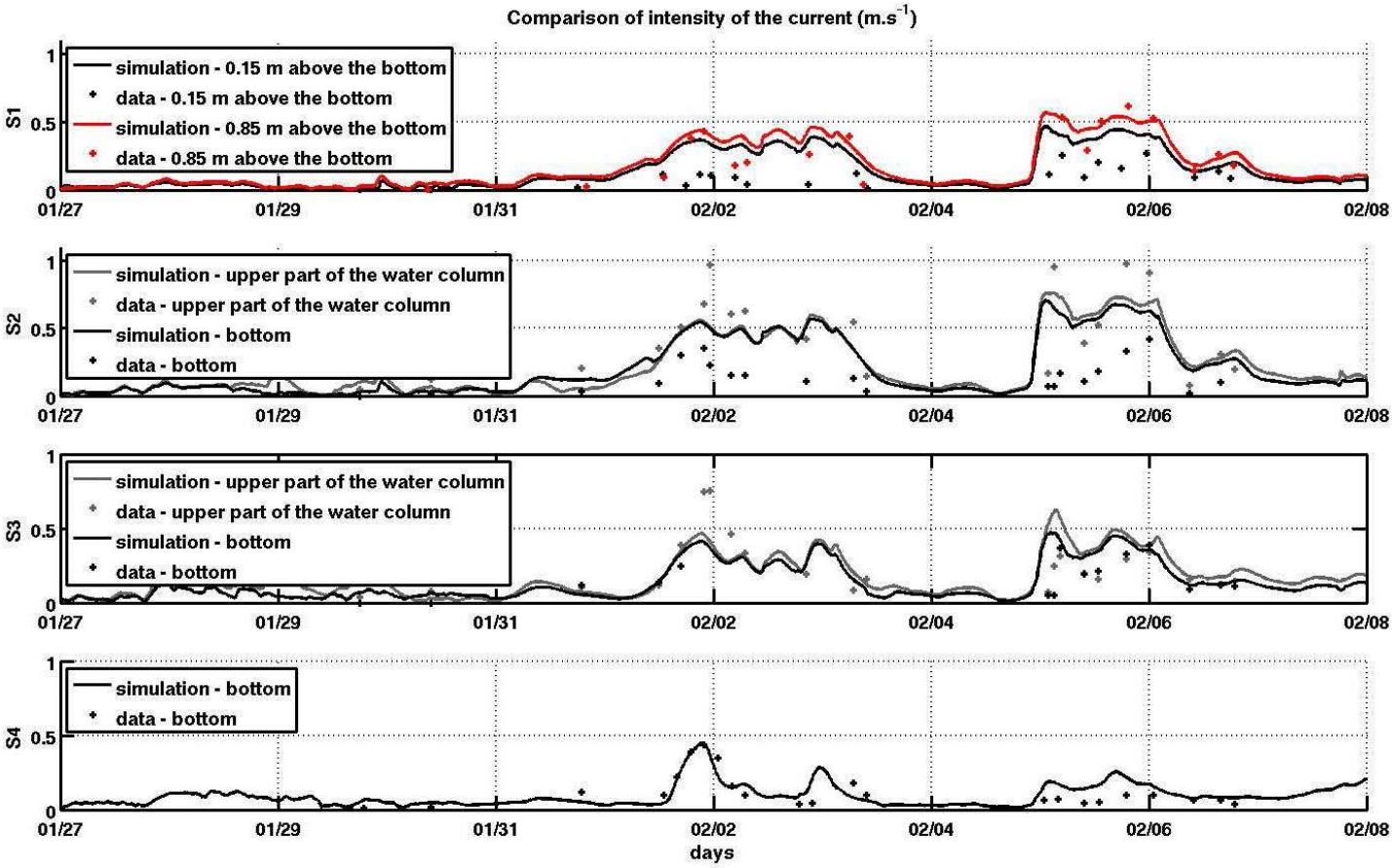


Figure 4. Comparison of current intensities between data and simulation at the four locations (S1, S2, S3 and S4) and at different depth depending on the position of the instruments. At S2 and S3, an average on the upper part of the water column (between -2.5 m and -0.5 m for S2 and between -3.5 and -0.5 m for S3) was performed for the grey points and lines.

A comparison with the measurements at the four locations is done to assess the performance of the model (figures 3 and 4). At S1, the comparison is performed at two depths: at 0.85 m above the bottom, simulation fits the data whereas at 0.15 m above the bottom, it strongly overestimates it. The simulated bottom friction must be underestimated at this point because the model gives quite similar results at these two different depths, whereas a decrease of current is observed. At S2, the current is stronger than in S1 and there is a good correlation between simulation and data, except near the bottom. In addition, the peaks of current are not well reproduced by our model. It seems that the vertical shear is misrepresented. At S3, the current is less strong than in S2 in both simulation and data. The peak is also underestimated in the simulation. This discrepancy can be linked to the the significant wave height which is underestimated during the peaks at S3 (figure 2b). Finally, at S4, the simulated bottom current is in agreement with the data for the first period and overestimates the data during the second period, when waves are also overestimated.

## 4. Discussion

### *4.1. Momentum balance*

In order to understand the role of waves and their mechanisms, we study the cross-shore distribution of the momentum terms (figures 5 and 6). Coriolis and Stokes-Coriolis forces are quite null at that scale and have not been represented. The barotropic longshore balance is led by the advection and the vortex force, the positive breaking acceleration and the vertical mixing. The forces associated to pressure gradient (pressure gradient and Bernoulli pressure head) are also very weak. Advection and vortex force compensate each other, and this cancellation is perfect in the entire vertical column (figures 6b and c). Thus, the longshore drift intensity is totally controlled by the balance between breaking acceleration and vertical mixing.

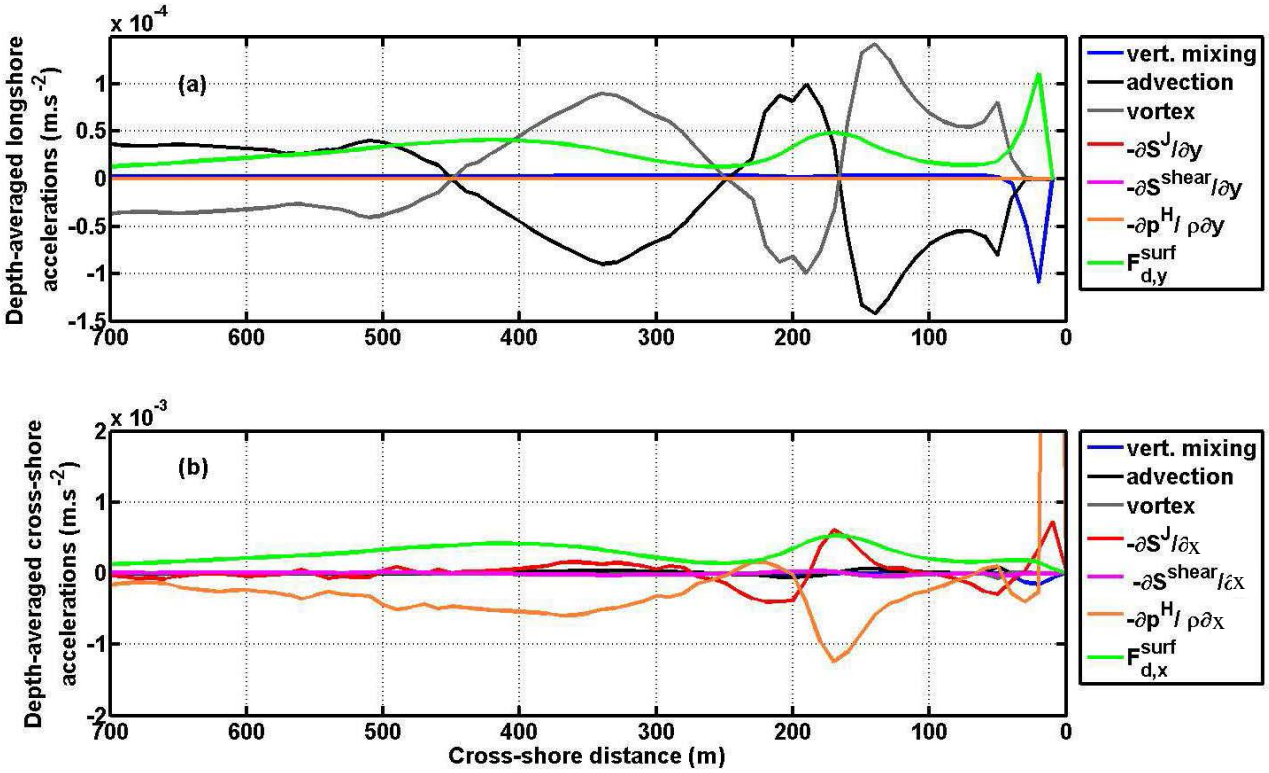


Figure 5. Cross-shore distribution of the depth-averaged longshore (a) and cross-shore (b) momentum terms ($m.s^{-2}$) at the storm apex on 1 February at 6p.m

Vertical mixing is dependent on the bottom stress and its depth-averaged value is only active and negative when the water depth is inferior to 3m of water depth (in the first 70 m and above the bar). The breaking acceleration is intensified at locations where the wave breaking dissipation is strongest (figure 6a): above the outer and inner bar. Besides, this force is confined in the two first meters of the water column, due to the penetration profile we have imposed (figure 6g). The vertical mixing force is also important at these locations near the surface trying to counterbalance the breaking acceleration and also in the inner trough near the bottom (figure 6a).

With an order of magnitude larger, the barotropic cross-shore acceleration is the result of the balance between three momentum terms (figure 5b): the breaking acceleration, the pressure gradient force (without the direct contribution of wave) and the wave- and shear-induced pressure gradient force. The wave-induced pressure gradient term is weaker than the pressure gradient force, with an opposite sign that tends to reduce its effect, except near the shoreline, where they both contribute to onshore strong cross-shore acceleration (figure 5b). The shear-induced term is null everywhere and negligible above the inner bar, created by some vertical circulation (figure 5b). At least, the advection has also a weak contribution, and it is no more cancelled by the barotropic vortex force which is null. Their vertical profiles in figure 6 show

that the breaking acceleration is intensified in the upper part of the water column (figure 6n). The vertical mixing force, even if it is null once depth-averaged, is maximum and negative near the surface, and maximum and positive near the bottom, in the entire cross-shore profile and above all, on the bars. The shear-induced term is non null near the bottom on the inner bar. At least, wave-induced pressure gradient and pressure gradient forces are depth-uniform.

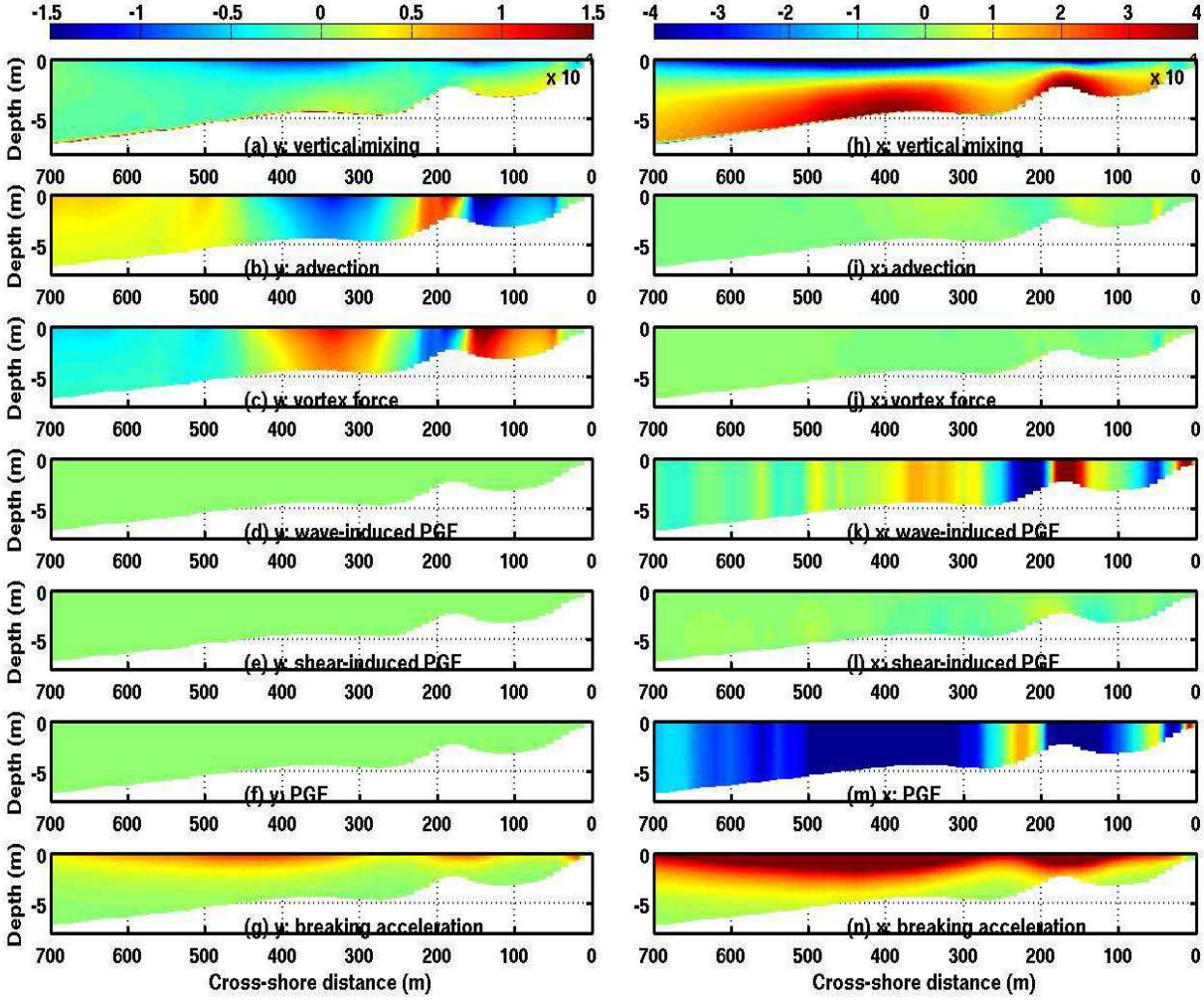


Figure 6. Vertical and cross-shore profiles of the cross-shore (x) and longshore (y) momentum terms (m.s$^{-2}$) at the storm apex on 1 February at 6 p.m.: (a) y vertical mixing, (b) y advection, (c) y vortex force, (d) y wave-induced pressure gradient force, (e) y shear-induced pressure gradient force, (f) y pressure gradient force, (g) y breaking acceleration, (h) x vertical mixing, (i) x advection, (j) x vortex force, (k) x wave--induced pressure gradient force, (l) x shear-induced pressure gradient force, (m) x pressure gradient force and (n) x breaking acceleration.

### *4.2. Importance of the roller effect*

We will assess the importance of the new parameter implemented, the roller effect by varying the value $\alpha_r$ in the model. When equal to 0, there is no wave roller and when equal to 1 means that all the energy of the primary wave is transferred to the roller. We also consider the value $\alpha_r$= 0.5.

When $\alpha_r$ increases, the two peaks of the total dissipation by wave and roller ratio ($\varepsilon^{tot} = (1-\alpha_r)\varepsilon^b + \varepsilon^r$)shift onshore and become slightly larger (Figure 7a). So a delay in the transfer of momentum between wave and current is generated. The setup is thus modified (Figure 7a) and is slightly

increased with a larger $\alpha_r$. When examining the barotropic values of the cross-shore and longshore velocities (Figure 7b), we note that they both increase everywhere and above all, on the bars. The peak of longshore current is also moved onshore. In the inner trough, the current is increased in the entire vertical column, since the amount of wave and roller dissipation and also the vertical mixing are increased (Figure 7c-f). When comparing to the measurements of the longshore velocity, the simulation with $\alpha_r$=1 is the best to reproduce the intense current in the inner trough..

The roller controls the cross-shore position of the longshore drift that is no longer confined on the external side of the inner bar, but can extend in the inner trough as the observations have pointed. So it is very important when dealing with surf zone to take into account this process (e.g., Church and Thornton, 1993, Reniers and Battjes, 1997, Ruessink et al. 2001).

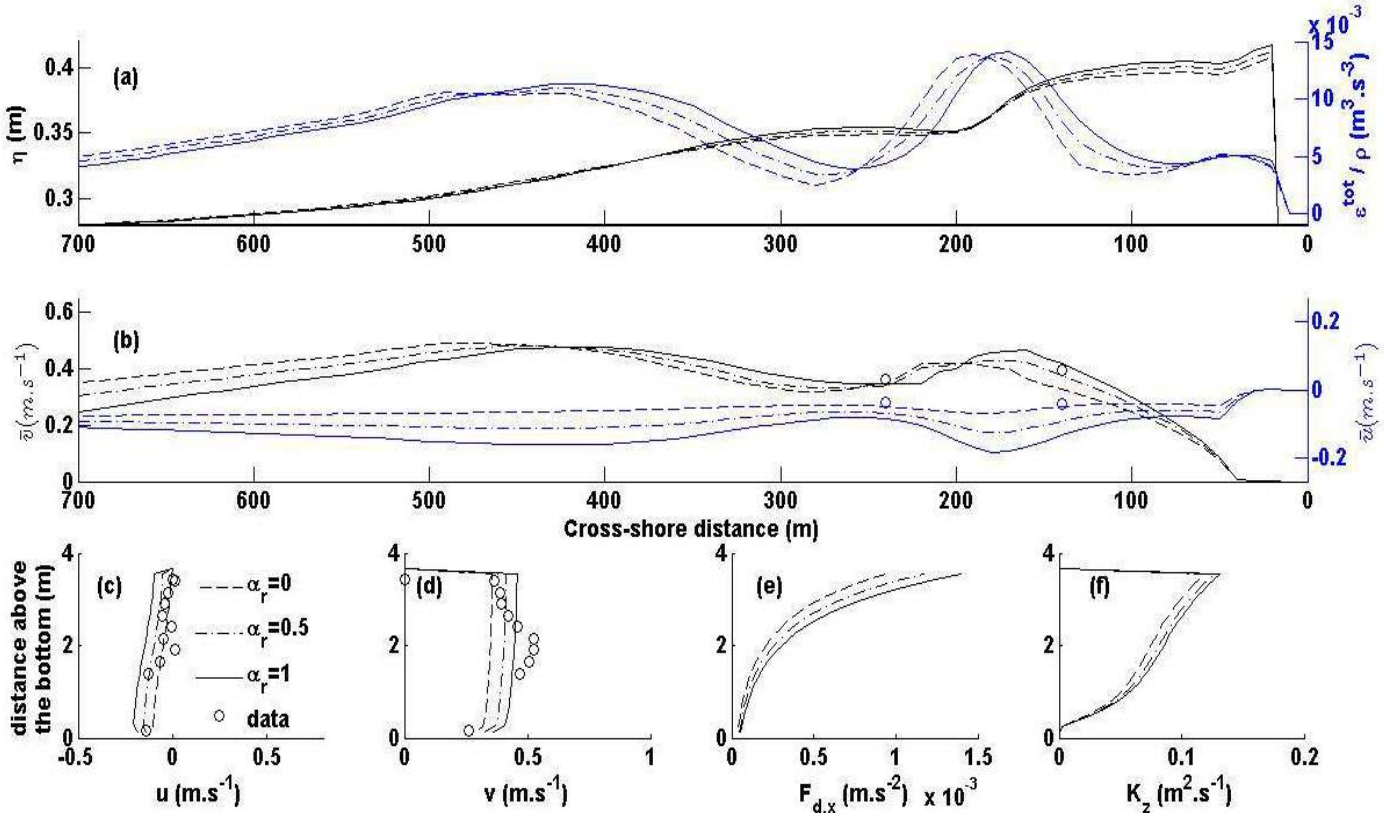


Figure 7. Influence of $\alpha_r$ values on the elevation (black) and the breaking dissipation rate (blue, $\varepsilon^{tot}/\rho$), the depth-averaged cross-shore (blue) and longshore (black) velocities (b), the vertical profiles at S2 of the cross-shore (c), longshore (d) velocities, the x breaking acceleration term (e) and the vertical mixing (f) at the storm apex (1 February at 6 p.m). Measured velocities at S2 and S3 are represented by circles.

### *4.3. Bottom stress parameterizations*

As previously noticed, bottom stress is crucial in the momentum balance. Besides, the simulated current pointed out a misrepresentation of the bottom drag. In the reference simulation, we used the drag law model that takes into account effects of waves and currents (Soulsby et al., 1995), with $z_0 = 100\,\mu m$ (equation 5). We thus will test different values of $z_0$ (50 µm and 1 mm) as well as other parameterizations: a linear drag model (equation 4) with µ = 0.004 and a quadratic model (equation 3) with $z_0 = 100\,\mu m$ (Figure 8). At last, a test is also performed where the bottom streaming is removed.

We observe that the intensity of the longshore current is directly changed, especially in the inner trough at S2. The smaller $z_0$ is, the bigger the longshore velocity is. The vertical profile of the cross-shore velocity is not modified, except near the bottom. Only with a strong $z_0$ equal to 1 mm, its shear is increased, and the bottom current is close to the data. The addition of streaming increases the momentum of current, and thus the barotropic longshore velocity. The parameterization of Soulsby et al., (1995) leads to increase the bottom friction, and so to decrease the intensity of current, when we compare the results with the ones of

the quadratic model. In conclusion, the parameterization of Soulsby et al. (1995), with $z_0 = 100\ \mu m$ was the most suitable to the data, at the four instruments (not shown). However, as shown in figure 4, the current overestimates the measurements near the bottom, the lonsghore velocity is not enough sheared and the cross-shore velocity is too strong compared to the data.
Several possibilities are considered to understand the source of discrepancy. The bathymetry is highly variable in this region, and even more during a storm, so it seems important to couple our model with a morphodynamic model. The second possible source of discrepancy can be linked to the fact that we have considered the beach uniform in the longshore direction.

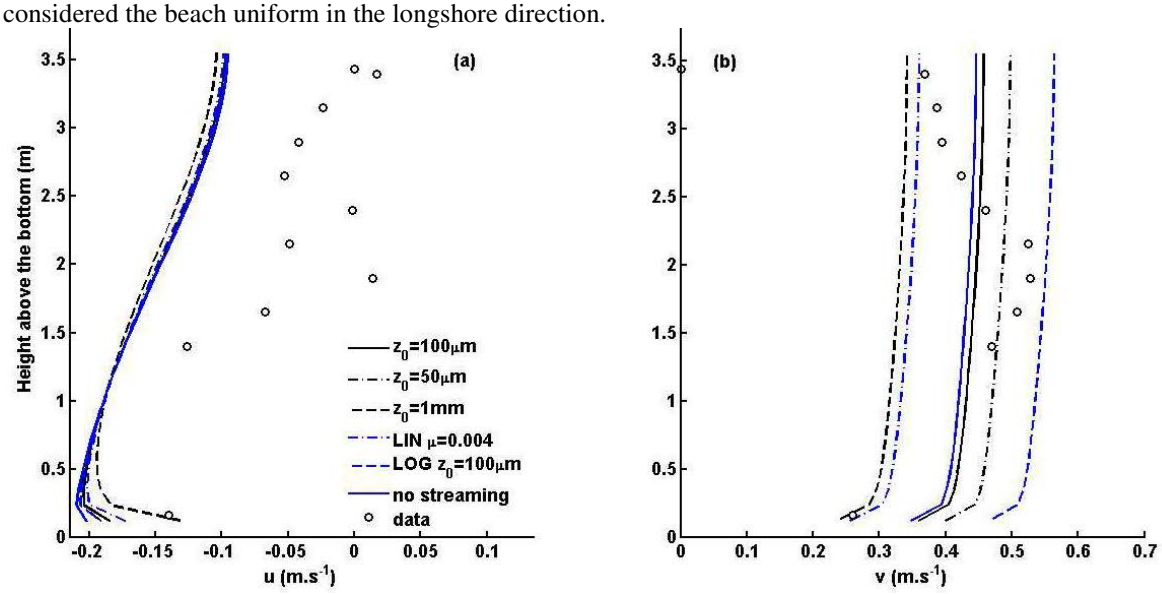


Figure 8 Comparison of the vertical profiles at S2 of cross-shore(a) and longshore(b) velocities at the storm rising stage, depending on the bottom parameterizations, at the storm rising stage on 1 February at 6 pm.

## 5. Conclusion

The field campaign on the Sète barred beach deployed during the winter 2009, recorded the circulation at several positions and depth for a storm in the beginning of February. A longshore drift developing offshore of the inner bar and also in the inner trough was thus measured. Implementing the 3D circulation model Symphonie with some additional parameterizations concerning the roller effects and the bottom friction on this situation permits to fit and validate our model in the surf zone and also to understand the role of the different processes. Besides, an analysis of the momentum terms at the apex shows the importance of the vertical mixing and the wave dissipation forces. Thereby, the roller influences the cross-shore position of the drift. The bottom friction is also of primary importance to control the intensity of the drift as well as the vertical profile of its cross-shore component. However, some overestimations of the simulated current are still noted at the peak and the bottom friction seems with the different parameterizations to be underestimated as well. In a context with a moving bedform in a highly variable environment, it is difficult to correctly represent the bottom current, without taking into account a morphodynamic model.

Thanks to its 3D nature and once associated with the sediment transport model (e.g., Ulses et al., 2008) and a morphodynamic model, it will offer a good representation of the sediment transport. Such a model will then be useful to assess the morphodynamical impacts of storms on the shoreface.

## Acknowledgements

We thank the persons involved in the field data, Microlit/Reliefs and the ANR Vulsaco. We thank also Cyril Nguyen, the POC crew for their assistance and the HPC@LR center. We thank the DREAL of Languedoc Roussillon for the LiDAR bathymetry. We acknowledge Météo-France for the ALADIN and ARPEGE for the model outputs. The Symphonie ocean model is developed by the SIROCCO group. Sources are available at http://sirocco.omp.obs-mip.fr/outils/Symphonie/Sources/SymphonieSource.htm

## References


Apotsos, A., B. Raubenheimer, S. Elgar, R. Guza, and J. Smith, 2007. Effects of wave rollers and bottom stress on wave setup, *Journal of Geophysical Research*, 112 (C02003).

Ardhuin, F., Rogers, E., Babanin, A., Filipot, J.F., Magne, R., Roland, A., Van Der Westhuysen, A., Queffeulou, P., Lefevre, J.M., Aouf, L., Collard, F., 2010. Semiempirical Dissipation Source Functions for Ocean Waves. Part I: Definition, Calibration, and Validation. *J. Phys. Oceanogr*. 40, 1917-1941.

Ardhuin, F., Rascle, N. and Belibassakis, K.A, 2008. Explicit wave-averaged primitive equations using a generalized Lagrangian mean. *Ocean Modelling* 20, 35-60.

Bennis, A.-C., Ardhuin, F. and Dumas, F., 2011. On the coupling of wave and three-dimensional circulation models: Choice of theoretical framework, practical implementation and adiabatic tests. *Ocean Modelling* 40, 260-272.

Bonneton, P., Chazel, F., Lannes, D., Marche, F. and Tissier, M. 2011. A splitting approach for the fully nonlinear and weakly dispersive Green-Naghdi model. *J. Comput. Phys*., 230, 1479-1498.

Certain, R., Meulé, S., Rey, V. and Pinazo, C., 2005. Wave transformation on a microtidal barred beach (Sète, France). *Journal of Marine Systems*, 38, 19-34.

Certain, R. 2002. Morphodynamique d'une côte sableuse microtidale à barres: le Golfe du Lion (Languedoc-Roussillon). *Phd thesis - Université de Perpignan Via Domitia.*

Church, J. and Thornton, E. 1993. Effects of breaking wave induced turbulence within a longshore current model, *Coastal Engineering*, 20. 1-28.

Denamiel, C. 2006. Modélisation hydrodynamique 3D en zone pré-littorale : Caractérisation des effets des houles de tempête sur la circulation océanique, *Phd thesis – Université Montpellier II*.

Estournel, C., F. Auclair, M. Lux, C. Nguyen, and P. Marsaleix, 2009. "Scale oriented" embedded modeling of the North-Western mediterranean in the frame of MFSTEP, *Ocean Sci*., 5 (2), 73-90.

Feddersen, F., Guza, R., Elgar, S, and Herbers T., 1998, Alongshore momentum balances in the nearshore. *Journal of Geophysical Research*, 103, 15.667-15.676.

Leredde, Y., C. Denamiel, E. Brambilla, C. Lauer-Leredde, F. Bouchette, and P. Marsaleix, 2007. Hydrodynamics in the gulf of aigues-mortes, nw mediterranean sea: In-situ and modelling data, *Continental Shelf Res.*, 2389-2406.

Longuet-Higgins, M.S. and Stewart R.W., 1962. Radiation stress and mass transport in gravity waves with application to surf beat, *Journal of Fluid Mechanics*, 13, 481-504.

Marsaleix, P., Auclair, F. and Estournel, C., 2009. Low-order pressure gradient schemes in sigma coordinate models: The seamount test revisited. Ocean Modelling 30, 169-177.

Marsaleix, P., Auclair, F., Floor, J. W., Herrmann, M. J., Estournel, C., Pairaud, I., Ulses, C. 2008. Energy conservation issues in sigma-coordinate free-surface ocean models. Ocean Modelling 20, 61-89.

Marsaleix, P. , Auclair, F., Estournel, C., 2006. Considerations on open boundary conditions for regional and coastal ocean models, *Journal of Atmospherics and Oceanic Technology,* 23, 1604-1613, doi:10.1175/JTECH1930.1.

McWilliams, J.C., Restrepo, J. and Lane, E., 2004. An asymptotic theory for the interaction of waves and currents in coastal waters, *Journal of Fluid Mechanics*, 511, 135-178.

Michaud, H., Marsaleix, P., Leredde, Y., Estournel, C., Bourrin, F., Lyard, F., Mayet, C., and Ardhuin, F., 2012. Three-dimensional modelling of wave-induced current from the surf zone to the inner shelf, *Ocean Science*, 8, 657-681.

Michaud, H., Leredde, Y., Estournel, C, Berthebaud E. and Marsaleix, P. 2013. Hydrodynamics during a typical winter storm in the Gulf of Aigues-Mortes (NW Mediterranean Sea) : In-situ measurements and numerical modelling. *Comptes rendus Geoscience, under review.*

Robin, N., Certain, R., Godon, C., Aleman, N. Gervais, M., Bouchette, F., Meulé, S., Barusseau, J.P., Ferrer, P., Balouin, Y., Brambilla, E., 2010. Caractérisation des profils de courants pendant des évènements de tempête sur une plage à barre rectiligne en milieu microtidal. *XIèmes Journées Nationales Génie Côtier - Génie Civil.*

Reniers, A., and J. Battjes, 1997 A laboratory study of longshore currents over barred and non-barred beaches., *Coastal Engineering*, 30, 1-22.

Reniers, A., J. Roelvink, and E. Thornton, 2004. Morphodynamic modeling of an embayed beach under wave group forcing, *Journal of Geophysical Research*, 109 (C1), doi:10.1029/2002JC001586.

Ruessink, B., Miles, J., Feddersen, F., Guza, R. and Elgar, S., 2001. Modelling the alongshore current on barred beaches. *Journal of Geophysical Research*, 106, 22.451-22.463.

Soulsby, R., M. Stive, H. de Vriend, J. Fredsoe, L. Hamm, C. Teisson, and J. Winterwerp, 1995. Bed shear stresses due to combined waves and current., *Advances in coastal morphodynamic*s, 4-20 4-23.

Svendsen, I. A., 1984. Wave heights and set-up in a surf zone, *Coastal Engineering*, 8, 303-329.

Tajima, Y., and O. Madsen, 2006. Modeling nearshore waves, surface rollers and undertow velocity profiles, *Journal of Waterway Port Coastal Ocean Eng*., 132, 429-438.

Tolman, H. A, 2008. mosaic approach to wind wave modeling. *Ocean Modelling* 25, 35-47.

Ulses, C., Estournel, C., Bonnin, J., Durrieu de Madron, X. and Marsaleix, P., 2008. Impact of storms and dense water cascading on shelf-slope exchanges in the Gulf of Lion (NW Mediterranean). *J. Geophys. Res*. 113.